A Double-Cable Polymer Acceptor Enables 20% Efficiency in Ternary Organic Solar Cells

Qin Tan, [a] Shijie Liang,*[a, b] Yang Cheng, [a] Lijuan Liu, [a] Haiyun Fan, [a] Bo Wang, [a] Chenhui Zhang,*[c] Chengyi Xiao and Weiwei Li*[a]

[a] Beijing Advanced Innovation Center for Soft Matter Science and Engineering & State Key Laboratory of Organic-Inorganic Composites, Beijing University of Chemical Technology, Beijing 100029, P. R. China. E-mail: liangshijie@bjtu.edu.cn; liweiwei@iccas.ac.cn

[b] School of Physical Science and Engineering, Beijing Jiaotong University, Beijing 100044, P. R. China. E-mail: liangshijie@bjtu.edu.cn

[c] College of Chemistry and Molecular Engineering, Peking University, Beijing 100871, P. R. China. E-mail: chhzhang@pku.edu.cn

Contents

1. Materials and measurements

Materials: All commercial chemicals (from *J&K Chemical*, *Alfa Aesar*, *TCI Chemical Co.*, and *Sigma-Aldrich*) were used as received. Proton nuclear magnetic resonance (^{1}H-NMR) spectra of intermedia products and monomers were recorded at 400 MHz on a *Bruker* AVANCE spectrometer. MALDI-TOF-MS spectra were determined on a *Bruker* BIFLEXIII mass spectrometer. Optical absorption spectra were recorded on a HITACHI U-2910 spectrometer with a slit width of 2.0 nm and a scan speed of 800 nm/min. Cyclic voltammetry was performed under an inert atmosphere at a scan rate of 0.1 V/s and 1 M tetrabutylammonium hexafluorophosphate in acetonitrile as the electrolyte, a glassy-carbon working electrode coated with samples, a platinum-wire auxiliary electrode, and an Ag/AgCl as a reference electrode. The atomic force microscopy (AFM) images were recorded using a Digital Instruments Nanoscope IIIa multimode atomic force microscope (*Bruker*) in tapping mode under ambient conditions. The GIWAXS data were obtained at 1W1A Diffuse X-ray Scattering Station, Beijing Synchrotron Radiation Facility (BSRF-1W1A). All-polymer binary components film sample were prepared by spin-coating CF/2-MN solutions on Si substrates; the D18:eC9 and ternary components are in the *o*-xy : CS_2 (v/v=5:4)/DIB solutions.

***J-V* and EQE:** The patterned ITO/glasses were ultra-sonicated for 10 min in detergent, deionized water, acetone, and isopropanol. Then, the substrates were treated in a UV-ozone chamber for 30 min. Next, the 2PACz[S1] (0.2 mg/mL in ethanol) were spin-coated onto the ITO glass substrates and then annealed at 80 °C for 3 minutes. The samples were then transferred into a N_2-filled gloved box. PM6:PYT-N mixture (1:1.2 in weight ratio, 13 mg/mL in chloroform with 10 mg/mL of 2-methoxynaphthalene as the additive) D18:e C9 (1:1.2) and D18:e C9:PYT-N (1:1.2:0.1) in *o*-xy:CS_2 (v/v=5:4), adding 4.5 mg/mL DIB as the additive, the concentration of D18 is 5 mg/mL. Then spin-coated at a speed of 2,600 rpm for 30 seconds to form a photoactive layer of about 100 nm. A thin layer of PNDIT-F3N (~10 nm) as the electron transport layer (ETL)

was spin-coated (1.1 mg/mL in methanol : formic acid = 100:1) on top of the photoactive layer. Finally, the silver electrode (Ag, 100 nm) was evaporated upon the photoactive layer under a high vacuum. Current density-voltage (*J-V*) characteristics were recorded inside a N_2-filled glove box under AM1.5G (100 mW/cm^2) illumination from a solar simulator (Enlitech model SS-F5-3A) with a standard silicon solar cell equipped with a KG5 filter (certificated by the National Institute of Metrology) and a Keithley 2400 source-measure unit. The active area of the cells was defined to be 0.032 cm^2 using a shadow mask. The EQE spectra were tested on a solar cell spectral response measurement system (QER3011, *Enli Technology Co. Ltd*.).

SCLC: The hole and electron mobility of binary or ternary films in OSCs were measured by space charge limit current (SCLC) measurement with the device configuration of ITO/PEDOT:PSS/active layer/MoO_3/Ag and ITO/ZnO/active layer/PDINN/Ag, respectively. All film samples were prepared with the same measurement of the solar cell devices by spin-coating solutions in an N_2-filled glove box and thermally annealed for 10 min. The thickness of the photoactive layers is ~100 nm. The hole/electron mobilities were calculated with the *Mott-Gurney* equation in the SCLC region (slope = 2 in log$J$ vs log$V$ plots) [S2]:

$$J = \frac{9}{8}\varepsilon_0\varepsilon_r\mu\frac{V^2}{L^3} \qquad \textbf{Equation S1}$$

Where ε_0 is the permittivity of the vacuum, ε_r is the dielectric constant of the polymer, and L is the thickness of the polymer layer.

Estimation of glass-transition temperature (T_g): The thermal transition was investigated through the exploitation of discernible shifts in the UV-visible absorption spectrum following the thermal annealing of a diverse array of pristine film samples. This spectral alteration is ascribed to the emergence of structured aggregates, which are intimately associated with the thermal behavior of the molecular constituents within the films. Beyond a certain annealing temperature threshold surpassing the transition temperature, a conspicuous alteration becomes readily apparent in the absorption spectrum. To perform a rigorous quantitative assessment, we employed a metric termed

the deviation metric (DM_T), which is computed as the sum of squared deviations in absorbance values between the as-cast and annealed film specimens[S3]:

$$DM_T = \sum_{\lambda_{min}}^{\lambda_{max}} [I_{RT}(\lambda) - I_T(\lambda)]^2 \quad \textbf{Equation S2}$$

Where λ is the wavelength, and λ_{min} and λ_{max} are the lower and upper bounds of the optical sweep, $I_{RT}(\lambda)$ and $I_T(\lambda)$ are the normalized absorption intensities of the as-cast (room temperature) and annealed films, respectively.

Photocurrent density versus effective voltage measurements: Photocurrent density (J_{ph}) versus effective voltage (V_{eff}) measurements[S4] were conducted with a comprehensive analysis based on the current density-voltage curves (voltage ranging from -1.5 to 1.5 V) obtained under both light and dark conditions. J_L is the light current density under the illumination of AM1.5G, 100 mW/cm^2 and J_D is the dark current density. $J_{ph} = J_L$-J_D, V_0 is the voltage when $J_L = J_D$, and V_{appl} refers to the applied voltage. $V_{eff} = V_0$-V_{appl}. Saturation current (J_{sat}) refers to the situation when free charges in the film are thrust out and collected by electrodes at a high V_{eff}.

Thermal stability measurements: Long-term thermal aging tests were performed by placing the unencapsulated devices on a hotplate at a constant temperature of 60 °C inside a nitrogen-filled glovebox. The photovoltaic parameters were recorded periodically under AM 1.5G (100 mW/cm^2) illumination for a total duration of 795 hours. The T_{80} lifetimes (the time required for the PCE to decay to 80% of its initial value) were estimated by linear extrapolation based on the steady-state degradation rates observed after the initial "burn-in" period.

2. Synthetic Procedure

M1 and M2 were synthesized according to the procedure reported in the literature[S5].

Synthesis of M3

A 250 mL double-mouth round bottom flask was selected as the reaction bottle. 1,4,5,8-Naphthalenetetracarboxylic dianhydride (1.2 g, 4.5 mmol) was weighed and 50 mL of anhydrous DMF was taken and placed in the reaction bottle. The 2-octyl-1-dodecylamine (1.34 g, 4.5 mmol) was dissolved in 10 mL of anhydrous DMF and placed in a constant pressure drop funnel to maintain the inert gas atmosphere in the reaction container. The mixture in the reaction flask was heated to 120 °C and dissolved for 30 minutes. The DMF solution of 2-octyl-1-dodecylamine was added dropwise. After stirring at 120 °C for 12 hours, the reactants were cooled to room temperature, and then extracted with brine and dichloromethane (100 mL), and dried with anhydrous $MgSO_4$. After removing the solvent by rotary vacuum evaporation, the crude product was transferred to a 100 mL single-mouth round-bottom flask, NH_4OAc (2.71 g, 0.045 mol) was added, and 50 mL AcOH was added as the reaction solvent. The mixture was heated to 100 °C and stirred for 4 hours to end the reaction. After the reaction was cooled to room temperature, it was extracted with water and chloroform (100 mL) and dried with anhydrous $MgSO_4$. After the solvent was removed by rotary vacuum evaporation, the crude product was purified by silica gel chromatography (chloroform:petroleum ether volume ratio 2:1 as eluent) to obtain M3 (1.35 g, yield 55%), which was a white solid. ^{1}H NMR (400 MHz, $CDCl_3$): δ (ppm): 8.90 (s, 1H), 8.81-8.74 (m, 4H), 4.14 (d, 2H), 2.03-1,93 (m, 1H), 1.42-1.17 (m, 32H), 0.92-0.77 (m, 6H).

Synthesis of M4

380 mg (0.29 mmol) M2 and 400 mg (0.73 mmol) M3 were added to a 100 mL reaction tube. Potassium iodide (50 mg, 0.38 mmol), potassium carbonate (200 mg, 1.18 mmol) and DMF (15 mL) were added and deoxygenated with nitrogen for 15 min. The mixture was reacted at 70°C for 15 h. After the reaction was cooled, it was extracted with dichloromethane and H_2O. Merge organic layer, $MgSO_4$ drying, filtration, silica gel column chromatography, dichloromethane / petroleum ether (1/2, v/v) elution, orange solid M4 (300 mg, yield 78 %) was obtained. ^{1}H NMR (400 MHz, $CDCl_3$): δ (ppm): 8.69 (s, 1H), 7.0 (d, 2H), 4.63-4.55 (m, 4H), 4.18-4.08 (t, 5H), 2.86-2.75 (dd, 5H), 1.39-0.78 (m, 136H).

Synthesis of M5

$POCl_3$ (0.1 mL) and N, N-dimethylformamide (DMF, 1.0 mL) were added to 1,2-dichloroethane (10 mL) and stirred at 0 °C for 30 min in N_2 atmosphere. Subsequently, the mixture was added dropwise to a 50 m L two-port flask containing M4 (0.3 g, 0.16 mmol) dissolved in 1,2-dichloroethane, and then stirred at 60 °C for 12 h. Add CH_3COONa aqueous solution and continue stirring overnight. The mixed solution was extracted by extraction method. CH_2Cl_2 and organic phase were dried with anhydrous sodium sulfate. After the solvent was removed, the crude product was purified by silica gel column chromatography and eluted with a petroleum ether / CH_2Cl_2 (v/v, 1:1) mixture to obtain a red solid M5 (0.29 g, 96 %). ^{1}H NMR (400 MHz, $CDCl_3$): δ (ppm): 10.13 (d, 2H), 8.72 (s, 4H), 4.68-4.59 (m, 5H), 4.17-4.09 (t, 5H), 3.22-3.16 (t, 4H), 2.38-2.32 (t, 2H), 1.96-1.87 (m, 6H), 1.34-0.80 (m, 137H).

Synthesis of M5

The dried pyridine (2.00 mL) was added to the 15 mL chloroform solution of M5 (120 mg, 0.06 mmol) and IC-Br (45 mg, 0.16 mmol) in a 100 mL three-necked round-bottom flask under nitrogen protection. The resulting mixture was stirred and heated to reflux for 12 h. After cooling to room temperature, the solvent was removed under vacuum conditions. After methanol precipitation and filtration, the crude product was separated and purified by silica gel column chromatography with petroleum ether / chloroform mixture (v/v = 3:1) as eluent to obtain black solid M6 (107 mg, yield 88%). ^{1}H NMR (400 MHz, $CDCl_3$): δ (ppm): 8.91-8.77(d, 2H), 8.73-8.65 (dd, 4H), 8.49-8.42 (d, 2H), 7.91 (s, 2H), 7.83-7.74 (t, 2H), 4.87-4.61 (d, 4H), 4.16-4.03 (m, 4H), 3.09-2.87 (d, 4H), 2.35 (s, 2H), 1.99 (s, 2H), 1.57-0.72 (m, 132H).

Synthesis of PYT-N

To an oven-dried Schlenk tube equipped with a magnetic stir bar and charged with M6 (45.0 mg, 0.019 mmol), T-Sn (7.96 mg, 0.019 mmol), Tris(dibenzylideneacetone)-dipalladium ($Pd_2(dba)_3$, 0.58 mg, 0.0006 mmol), Tri(*o*-tolyl)phosphine P(*o*-tol)$_3$, 0.88

mg, 0.0024 mmol), and toluene (1.5 mL). The tube was freeze-pump-thawed three times and backfilled with nitrogen. The reaction was stirred at room temperature for 3 min, and then heated at 110 °C for 12 h. The reaction mixture was cooled to ambient temperature,. Chlorobenzene was added, precipitated in methanol, filtered in the fiber filter cartridge, and the filtrate was discarded. The fiber filter cartridge was successively extracted with methanol, petroleum ether and dichlorosol. After concentration, PYT-N was obtained by methanol precipitation and drying. (38 mg, yield 88%).

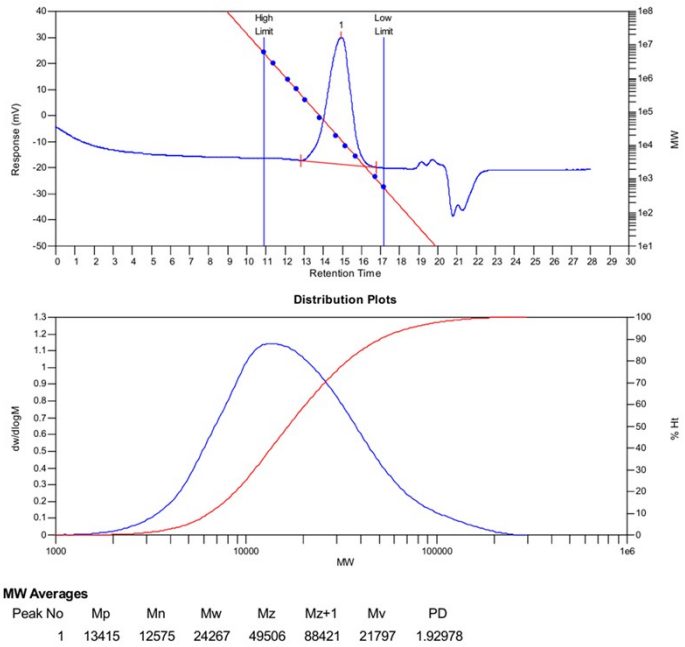

Fig. S1 GPC spectrum of PYT-N.

.

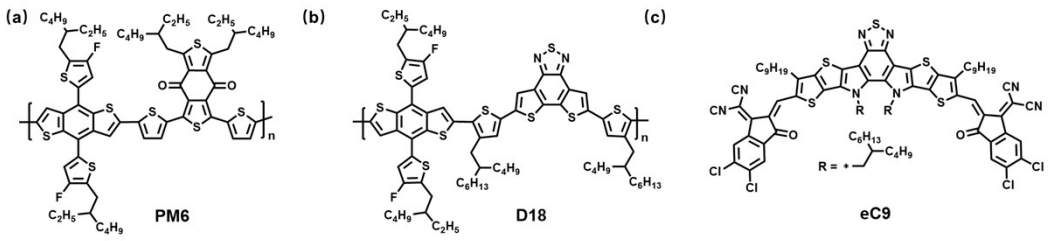

Fig. S2 Chemical structure of (a) D18, (b) PM6 and (c) eC9.

3. CV Spectra

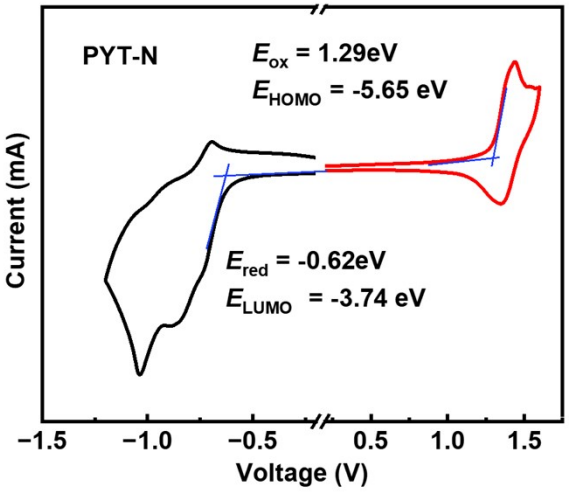

Fig. S3 Cyclic voltammograms of PYT-N.

4. Characterization of OSCs

Table S1. Photovoltaic performance of 6 devices based on PM6:PYT-N fabricated from CF with 10 mg/mL of 2-MN as additive annealed at 100 ºC for 10 min.

Active layer	V_{OC} (V)	J_{SC} (mA cm^{-2})	FF (%)	PCE (%)
PM6:PYT-N	0.903	20.76	75.33	14.14
PM6:PYT-N	0.903	21.42	75.08	14.53
PM6:PYT-N	0.902	21.38	74.80	14.43
PM6:PYT-N	0.908	22.43	73.86	14.43
PM6:PYT-N	0.908	21.61	73.94	14.49
PM6:PYT-N	0.904	21.19	74.57	14.27
average	0.904±0.002	21.46±0.55	74.59±0.59	14.38±0.14

Table S2. Photovoltaic performance of 6 devices based on D18:eC9 fabricated from *o*-xy:CS_2 (5:4) with 4.5 mg/mL of DIB as additive annealed at 90 ºC for 5 min.

Active layer	V_{OC} (V)	J_{SC} (mA cm^{-2})	FF (%)	PCE (%)
D18: eC9	0.858	29.38	77.92	19.65

D18: eC9	0.859	29.46	78.62	19.91
D18:eC9	0.857	28.14	79.01	19.06
D18:eC9	0.858	28.93	79.33	19.71
D18:eC9	0.855	28.88	77.80	19.23
D18:eC9	0.858	28.39	78.42	19.12
average	0.857±0.001	28.54±0.30	78.51±0.59	19.30±0.18

Table S3. Photovoltaic performance of 6 devices based on D18:eC9 fabricated from *o*-xy:CS_2 (5:4) with 4.5 mg/mL of DIB as additive annealed at 90 ºC for 5 min.

Active layer	V_{OC} **(V)**	J_{SC} **(mA cm^{-2})**	**FF (%)**	**PCE (%)**
D18:eC9:PYT-N	0.861	29.19	80.54	20.26
D18:eC9:PYT-N	0.860	29.05	80.27	20.05
D18:eC9:PYT-N	0.861	28.99	80.34	20.04
D18:eC9:PYT-N	0.859	29.00	80.43	20.05
D18:eC9:PYT-N	0.860	29.03	80.22	20.02
D18:eC9:PYT-N	0.861	29.17	80.32	20.17
average	0.860±0.008	29.08±0.08	80.35±0.11	20.11±0.08

5. Energy Loss Analysis and SCLC Measurements

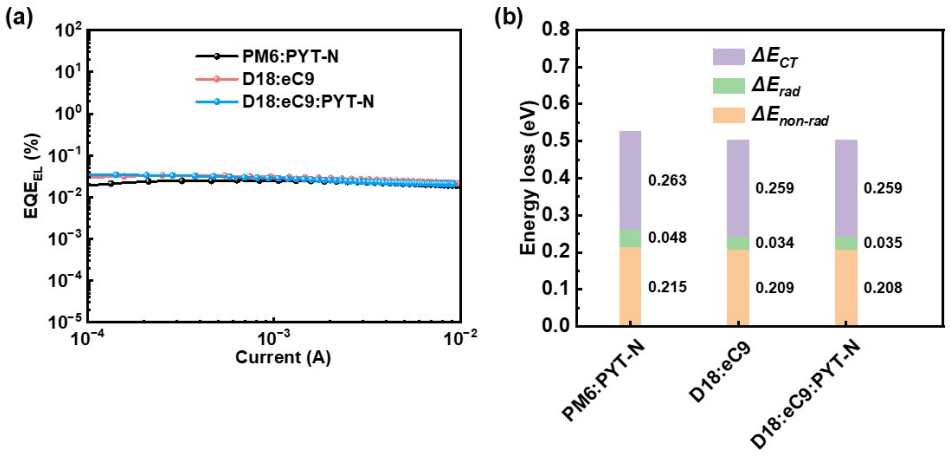

Fig. S4 Quantitative energy loss analysis of the studied devices.(a) External quantum efficiency of electroluminescence (EQE_{EL}) as a function of injected current for PM6:PYT-N, D18:eC9, and D18:eC9:PYT-N based devices. (b) Summary of the energy loss components.

Table S4 Detailed energy loss parameters and electroluminescence properties of the binary and ternary devices.

Active layers	E_g (eV)	E_{loss} (eV)	V_{oc}^{sq} (eV)	V_{oc}^{rad} (eV)	ΔE_1 (eV)	ΔE_2 (eV)	ΔE_3 (eV)	EQE_{EL} ($\times 10^{-4}$)
PM6:PYT-N	1.450	0.526	1.187	1.139	0.263	0.048	0.215	2.50
D18:eC9	1.374	0.502	1.115	1.081	0.259	0.034	0.209	3.10
D18:eC9:PYT-N	1.380	0.502	1.121	1.085	0.259	0.035	0.208	3.20

Note: $E_{loss}=E_g-qV_{OC}$. $\Delta E1$ is the radiative recombination loss above the bandgap; ΔE_2 is the radiative recombination loss due to the absorption tail below the bandgap; ΔE_3 is the non-radiative recombination loss calculated by $\Delta E_{non-rad}=-kTln(EQE_{EL})$.

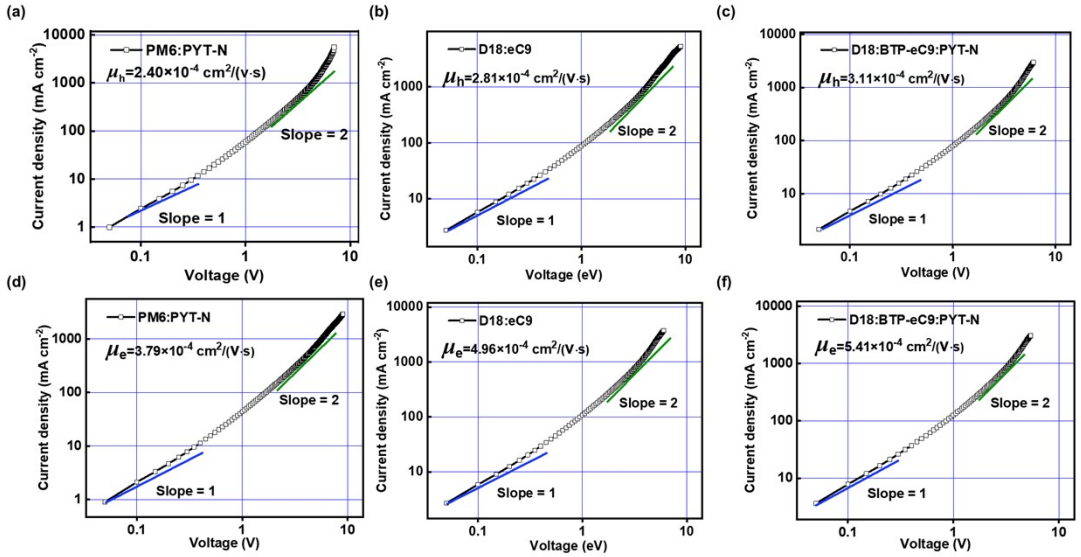

Fig. S5 (a-c) Hole-only and (d-f) electron-only devices for these blends.

Table S5. Charge carrier mobilities determined by SCLC measurements.

Materials	μ_h [$\times10^{-4}$ cm^2 V^{-1} s^{-1}]	μ_e [$\times10^{-4}$ cm^2 V^{-1} s^{-1}]	μ_e/μ_h
PM6:PYT-N	2.40	3.79	1.57
D18:eC9	2.81	4.96	1.74
D18:eC9:PYT-N	3.11	5.41	1.73

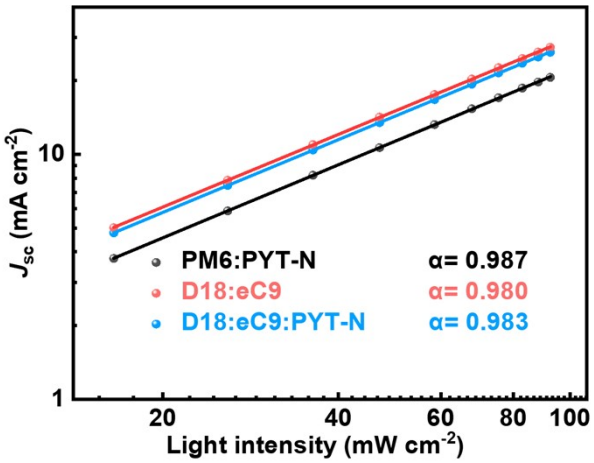

Fig. S6 J_{SC} versus light intensity for PM6:PYT-N,D18:eC9 and D18:eC9:PYT-N.

6. AFM measurements

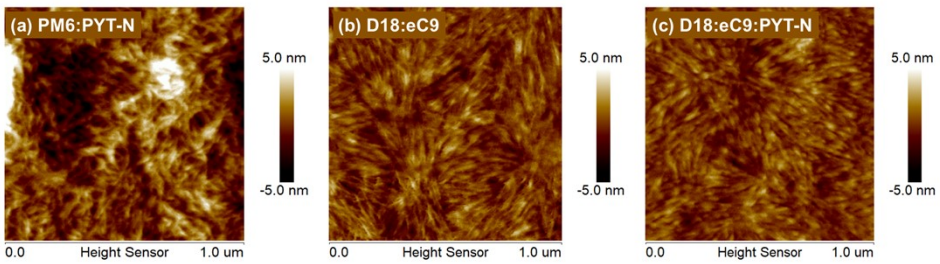

Fig. S7 Atomic force microscope height phase diagrams of (a) PM6:PYT-N, (b) D18:eC9 and (c) D18:eC9:PYT-N films.

Table S6 Crystallographic parameters of three blend films.

Active layers	IP (100)			OOP (010)		
	q **(Å^{-1})**	***d*** **(Å)**	**CCL^a (Å)**	***q*** **(Å^{-1})**	***d*** **(Å)**	**CCL^a (Å)**
PM6:PYT-N	0.288	21.81	48.33	1.651	3.80	15.53
D18:eC9	0.293	21.44	76.41	1.668	3.76	30.40
D18:eC9:PYT-N	0.291	21.59	79.64	1.679	3.74	21.02

^{a}CCL = 2π*k*/*fwhm*, where *k* is a shape factor (here is 0.9).

7. NMR and MS Spectra

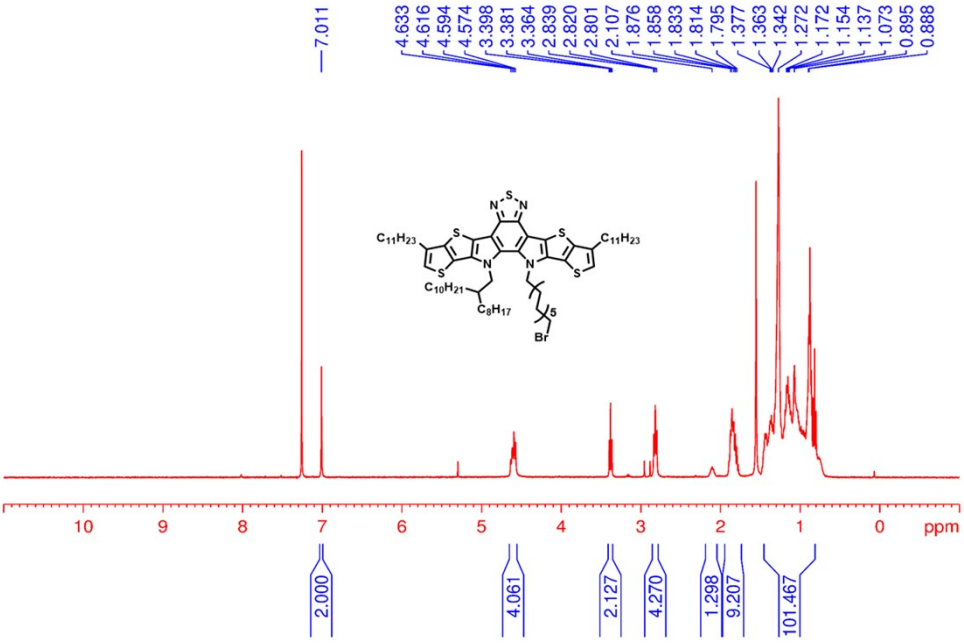

Fig. S8 ^{1}H-NMR spectrum of the M2 recorded in $CDCl_3$.

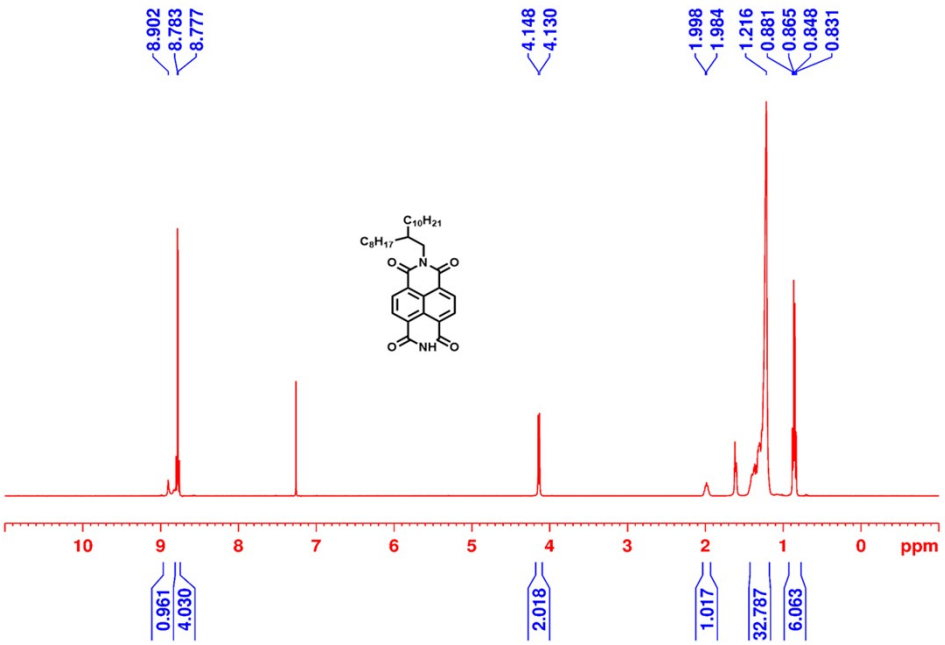

Fig. S9 ^{1}H-NMR spectrum of the M3 recorded in $CDCl_3$.

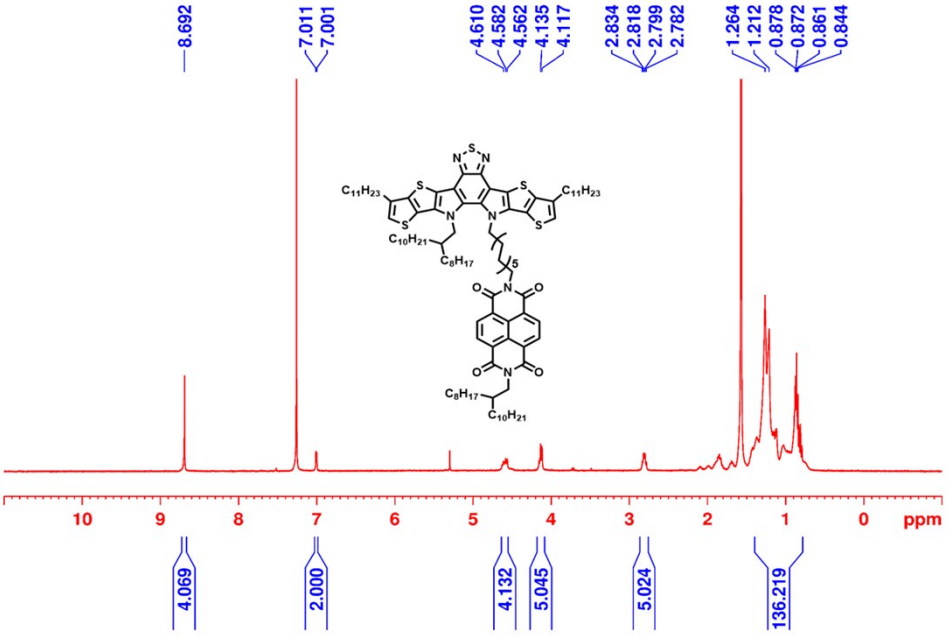

Fig. S10 ^{1}H-NMR spectrum of the M4 recorded in $CDCl_3$.

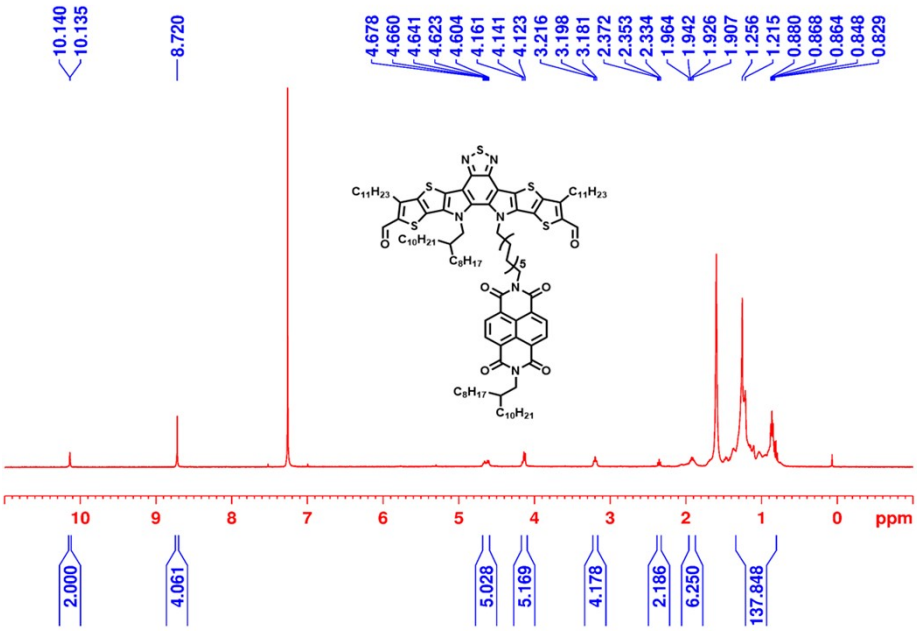

Fig. S11 ^{1}H-NMR spectrum of the M5 recorded in $CDCl_3$.

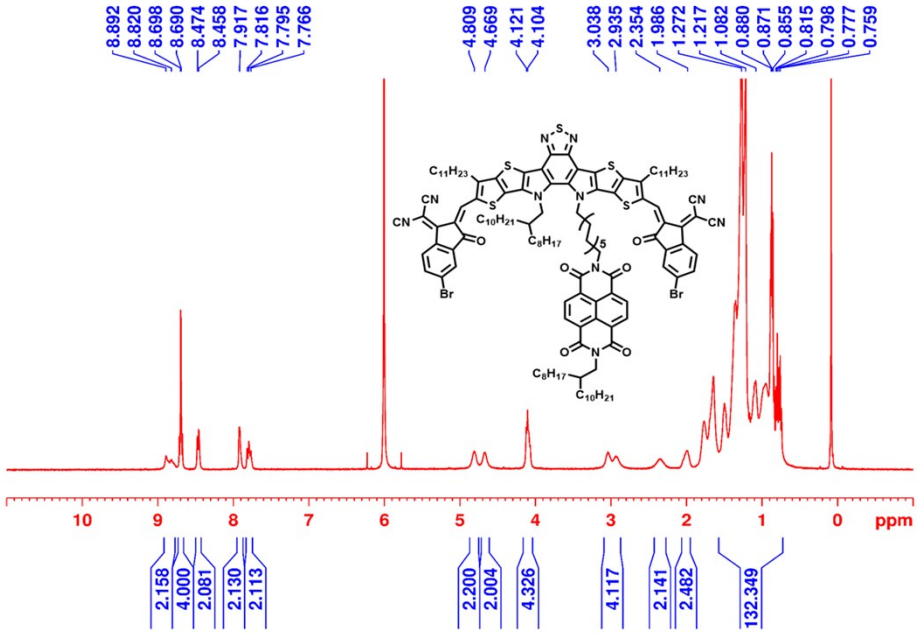

Fig. S12 ^{1}H-NMR spectrum of the M6 recorded in $CDCl_3$.

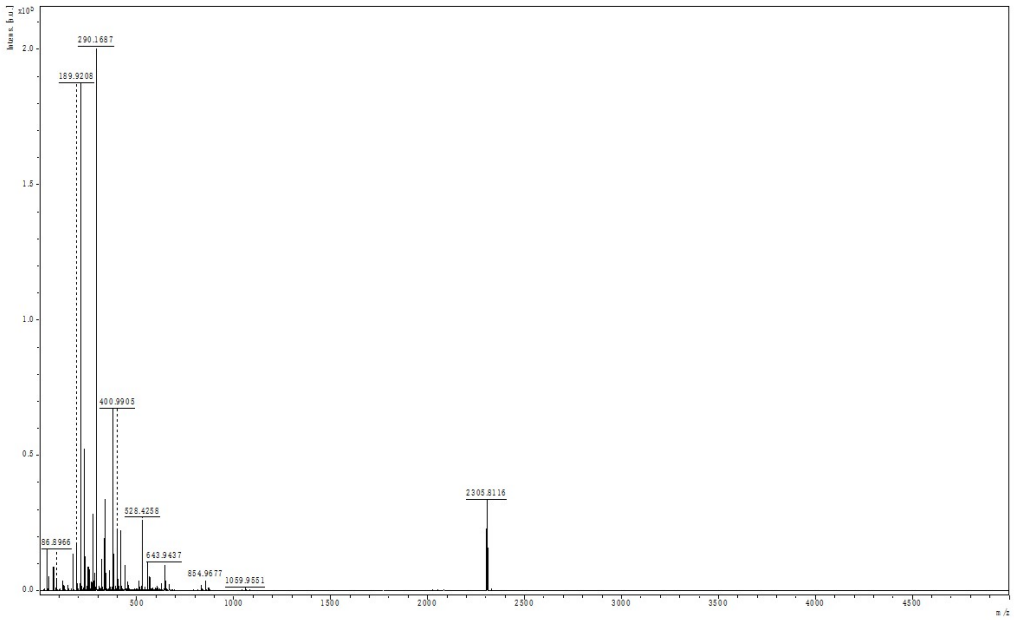

Fig. S13 High-resolution MALDI-TOF-MS spectrum of M6.

8. Reference

[S1] Y. Lin, Y. Firdaus, F. H. Isikgor, M. I. Nugraha, E. Yengel, G. T. Harrison, R. Hallani, A. El-Labban, H. Faber, C. Ma, X. Zheng, A. Subbiah, C. T. Howells, O. M. Bakr, I. McCulloch, S. D. Wolf, L. Tsetseris, T. D. Anthopoulos, *ACS Energy Lett.* **2020**, *5*, 2935.

[S2] a) B. Pukánszky, F. Tüdõs, *Makromol. Chem., Macromol. Symp.* **1990**, *38*, 221; b) S. Wu, *J. Polym. Sci., Part C: Polym. Symp.* **2007**, *34*, 19; c) A. Leclair, B. D. Favis, *Polymer* **1996**, *37*, 4723.

[S3] S. E. Root, M. A. Alkhadra, D. Rodriquez, A. D. Printz, D. J. Lipomi, *Chem. Mater.* **2017**, *29*, 2646.

[S4] V. D. Mihailetchi, L. J. Koster, J. C. Hummelen, P. W. Blom, *Phys. Rev. Lett.* **2004**, *93*, 216601.

[S5] Chen. S, Zhu. S, Hong. L, *Angew. Chem. In. Ed.* **2024**, *63*, e202318756.